CrystEngComm

Accepted Manuscript

ROYAL SOCIETY OF CHEMISTRY

www.rsc.org/crystengcomm

Enhanced features of Li_2CO_3 sputtered thin films induced by thickness and annealing time.

Lander Rojo,*[,†,‡] Irene Castro-Hurtado,[†,‡] Maria C. Morant-Miñana,[‡] Gemma García Mandayo,[†,‡] and Enrique Castaño[†,‡]

CEIT, Paseo Manuel de Lardizabal 15, 20018 Donostia-San Sebastián, Spain, and CIC microGUNE, Goiru Kalea 9 Polo Innovación Garaia, 20500 Arrasate-Mondragón, Spain

E-mail: lrojo@ceit.es

Phone: +34 943 212 800 . Fax: +34 943 213 076

Abstract

Li_2CO_3 sputtered films of 300 nm have been subjected to physical and electrochemical characterization methods to analyze the influence of annealing treatment at 600 °C during 2 h, 6 h, 12 h and 18 h on the microstructure, surface and conductivity. X-ray diffraction (XRD), Fourier transform infrared spectroscopy (FT-IR), atomic force microscopy (AFM) and electrochemical impedance (EIS) have been used for this purpose. XRD and FT-IR have illustrated the evolution of the microstructure with the annealing time. AFM analysis has shown the growth of new Li_2CO_3 particles that increase with the annealing time presenting a maximum diameter of 16.8 μm without compromising the continuity of the films. EIS measurements have described a fall in the activation energy of Li_2CO_3 thin films presenting a minimum around 1.18 eV. The results concerning the activation energy of the films have concluded an improvement

*To whom correspondence should be addressed
†CEIT
‡CIC microGUNE

regarding the results obtained previously in Li_2CO_3. These results serve to understand and optimize the behaviour of Li_2CO_3 thin films in gas sensors, fuel cells or Li^+ ion batteries.

Introduction

Lithium carbonate (Li_2CO_3) as an ionic conductor, has diverse uses in electrical devices. It can be employed as sensing electrode or solid electrolyte of CO_2 electrochemical sensors. Despite its employment is not so extended as other carbonates, the literature present Li_2CO_3 as a reliable material for these purposes.[1–5] Moreover, this carbonate has another scope of applicability in, for instance, the molten carbonate fuel cell (MCFC) field and Li^+ ion batteries. Li_2CO_3 has big influence on the life of this kind of batteries. Whether as an alternative to graphite anode,[6] an additive[7] or as a product due to the oxidation of the electrolyte, the reversibility of this carbonate contributes to the premature death of this kind of batteries.[8] Despite its wide uses, there are few studies focused on its characterization.[6,9,10] This is an indispensable work because the performance of any device under different conditions can be affected by several factors related to the behaviour of the materials it is made of.

A previous work of the group,[11] was focused on understanding the influence of annealing temperature on properties of Li_2CO_3 thin films. 200 nm Li_2CO_3 films were fabricated and subjected to different annealing treatments. The optimal annealing temperature for Li_2CO_3 films was 600 °C because more crystalline, uniform and reproducible surfaces were obtained with an activation energy of 1.5 eV at temperatures below 350 °C. An impedance increase was observed when the films were tested above 350 °C affecting the high temperature behaviour of Li_2CO_3 thin films. Two factors could be responsible of this behaviour: an inadequate film thickness and an insufficient annealing time. For this reason, in this work, a thicker film of Li_2CO_3 has been fabricated and longer stabilization times has been used. Samples annealed during 2 h, 6h, 12 h and 18 h have been compared to observe the influence of the annealing time on Li_2CO_3 thin films. These results serve to understand and optimize the behaviour of

lithium carbonate thin films in gas sensors, fuel cells or Li^+ ion batteries.

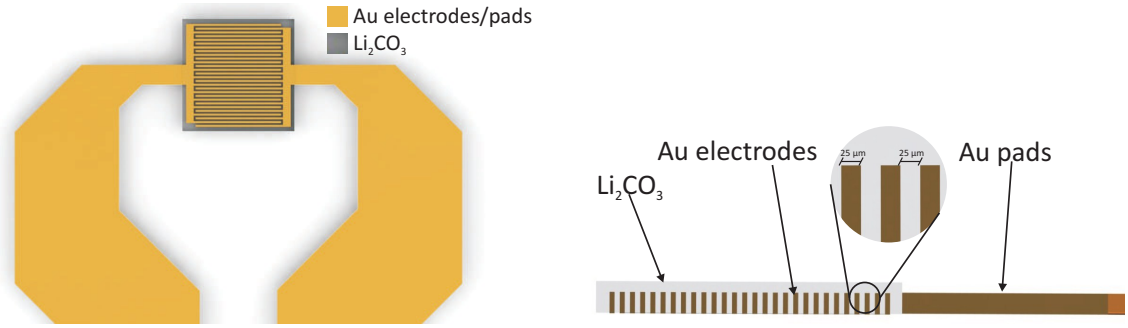

(a) (b)

Figure 1: Representation of the Li_2CO_3 sputtered cell.(a) Top view of the Li_2CO_3 over Au interdigitated electrodes and (b) cross-section of the electrochemical cell.

Experimental

Li_2CO_3 layers fabrication

Li_2CO_3 thin films deposition were performed from a high purity Li_2CO_3 target (99.9 % Testbourne) by RF magnetron sputtering (Pfeiffer Classic 500) on a polished α-Al_2O_3 substrate with a reported by the manufacturer surface roughness of 5 nm (Kyocera) and in an entire CO_2 atmosphere. The masks used for the photolithographic process were manufactured by Microlithography Services. The mask consists on a polyester based 007" thick film and a black area that is the photosensitive coating after it has been developed through the processing stage. The Li_2CO_3 layer was patterned as a square of 1.5 mm x 1.5 mm with an average thickness of 300 nm measured with a KLA Tencor profilometer. The complete fabrication process of sputtered Li_2CO_3 thin films is described in previous research reports of the group.[11] Due to the high ionic conduction temperature of Li_2CO_3, a thermal treatment temperature of 600 °C was established to stabilize the microstructure of Li_2CO_3 film and avoid any possible phase transition during high temperature operation. The samples were annealed at 600 °C during 2h, 6h, 12h and 18h to study the influence of the annealing

time. All the thermal treatments were performed in a ATV PEO 601 furnace and in CO_2 atmosphere. The reason for using this atmosphere in the deposition and in the annealing treatment steps was to prevent the co-deposition of Li_2O produced by the decomposition of Li_2CO_3.[12]

Electrochemical cell fabrication

Regarding EIS measurements, it is necessary to include thin film electrical connections and a heater. An integrated electrochemical cell consisting of Au electrodes and a Pt heater is formed. The Au electrodes and the Li_2CO_3 layer are illustrated in Figure 1. A 200 nm-thick Pt heater was deposited by DC magnetron sputtering (Edwards coating system E306A) on the bottom part of the Al_2O_3 substrate. The heater provides the different temperatures to the Li_2CO_3 in this EIS study. Following this step, 200 nm-thick Au interdigitated electrodes with a finger width of 25 μm were deposited by RF magnetron sputtering (Edwards coating system E306A) on the top part of the Al_2O_3 substrate. The metalic layers were deposited in an Ar atmosphere. Afterwards, an annealing treatment of 600 ^{o}C was applied for 2 hours to stabilize both metallic layers in a synthetic air atmosphere. Finally, in order to get the electrochemical cell, the Li_2CO_3 thin film is deposited using the fabrication process described above.

Characterization methods

The crystallographic structure of the Li_2CO_3 films before and after the thermal treatments was analyzed by X-ray diffraction (XRD) by means of a Philips XPERT MRD diffractometer in a glancing angle configuration ($\omega = 2\,^{o}$ and Cu $K_{\alpha 1}$ $= 1.54059$ Å). The diffraction patterns were obtained in the 20 ^{o} - 80 ^{o} range with a size of 0.015 ^{o} a time per step of 6.5 seconds. FT-IR measurements were collected using Perkin-Elmer Spectrum 100 spectrometer with Universal Attenuated Total Reflectance (UATR) accessory. Spectra were recorded over the range 4000-650 cm^{-1}, with a resolution of 4 cm^{-1} and 4 accumulations. A JPK NanoWizard

atomic force microscope in the intermittent contact mode using a Silicon tip (r < 10 nm; Aspect ratio < 6:1) with a force constant of 40 Nm^{-1} and a resonant frequency of approximately 300 kHz was employed to study the topography of the material under test. In addition to this, a Quanta 3D field-emission scanning electron microscope (FE-SEM) system supplied by FEI was used to study the topography. The micrographs were obtained using accelerating voltages of 15 kV. The EIS analysis was performed with a Solartron 1260 frequency response analyzer in the frequency range of 0.1 Hz - 4 MHz and an applied amplitude of 200 mV. The data was obtained and processed with Zview and Zplot tools. Afterwards, the obtained impedance patterns were fitted with an equivalent circuit in order to quantitatively analyze the obtained results. These measurements were performed in a controlled CO_2 atmosphere by means of a computer-controlled flow of 200 sccm from Bronkhorst Hi-Tech, using certified bottles of 99.9 % of CO_2 provided by Air Liquide and inside a sealed stainless steal chamber.

Results and discussion

Continuous Li_2CO_3 films of 300 nm thickness over several mm were prepared depending on the sputtering time as revealed by profilometer. These films are designed for working at high temperature and therefore, an annealing temperature of 600 °C was established for Li_2CO_3 films. Appart from the annealing temperature, the annealing time have strong influence on the microstructure of the material. For this purpose, XRD and FTIR techniques have been used to analyze the evolution of Li_2CO_3 microstructure with the annealing time as Figures 2 and 3. All the observed peaks corresponding to Li_2CO_3 and their orientations are highlighted in the picture as well as the rest of the peaks generated from the Al_2O_3 substrate. Due to the low intensity of the Li_2CO_3 peaks, some of them are not easily observed mainly at short annealing times. The obtained Bragg peaks are characteristics of a monoclinic structure with (002) preferred orientation (checked against ICDD:00-022-1141). Observing the intensity of the peaks, the (-110), (111), (-311) and (021) peaks remain practically unaltered with the

annealing time. However, a change with the annealing time can be noticed in the intensity of the peaks (-202), (-112) and (002). Peaks (-202) and (-112) are hardly observable in the as-deposited samples and the samples treated during 2 hours. The intensity of the peak (002), on the contrary, suffers a more gradual increase between samples. This means that the samples are more crystalline with longer annealing times. Interestingly, the peak (020) disappears with the annealing time. However, regarding the crystallinity, the longer annealing time the more crystalline films are obtained. Finally, the absence of Li_2O peaks confirms the high purity of Li_2CO_3 films.

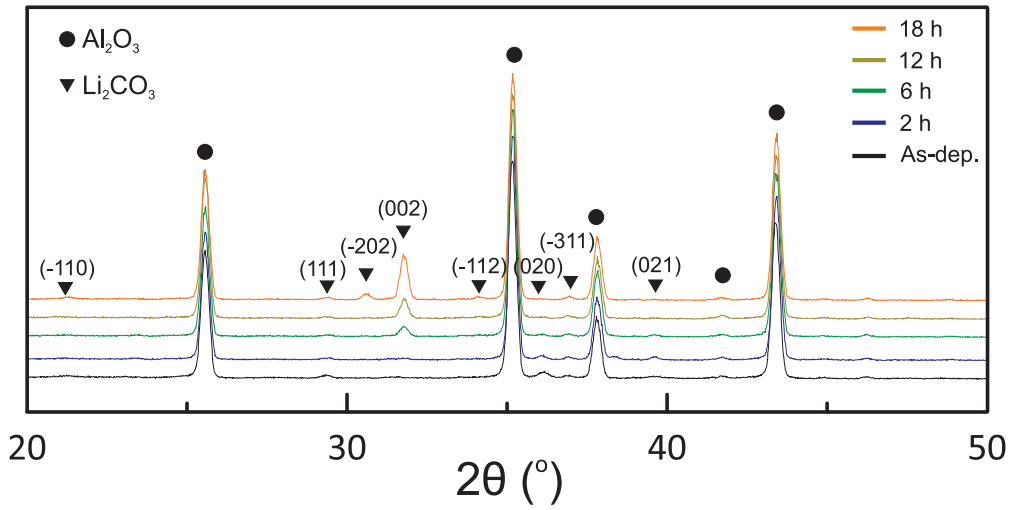

Figure 2: Li_2CO_3 diffraction pattern of as-deposited samples and samples annealed at 600 C during 2h, 6h, 12h and 18 h.

Figure 3 shows the absorption spectra of Li_2CO_3 samples obtained with FTIR technique for the different applied thermal treatments. In general, the absorption bands located between 1800 cm^{-1} and 700 cm^{-1} are attributed to the vibration of the CO_3^{2-} ion.[9,13] The clearly differentiated twofold absorption band around 1500 cm^{-1}, due to asymmetric stretching vibrations (υ_3) of C=O, is characteristic in Li_2CO_3 compounds.[8] A weak band around 1100 cm^{-1} is also observed due to symmetric stretching vibrations (υ_1) that are more observable in Raman Spectroscopy.[9,14] The carbonates IR spectra show a narrow band around 860 cm^{-1} representing the bending out of plane (υ_2) of the CO_3^{2-} ion. After 2 hours of thermal treatment, this band moves to higher wavenumber which is in agreement with the general

trend that indicates the higher crystallinity of the films with increasing annealing time.[15] Moreover, the carbonate spectra starts showing a new band located at 700 cm^{-1}. This could be atributed to bending in plane vibrations (υ_4) of Li_2CO_3.[14] The appearance of this band is explained by the splitting of the υ_4 band observed in other carbonates. The bands located at 631 cm^{-1} and below are associated to the Al_2O_3 substrate as the Figure 7 in the SI illustrates and remains unaltered during the annealing treatment process. Unlike other carbonates, as Li_2CO_3 only has one polymorph it indicates that no phase transformation takes place and the carbonate crystallize in a monoclinic structure as evidenced also in XRD analysis. In contrast to as-deposited samples, the flat characteristic within 4000-1750 cm^{-1} region indicates the absence of OH- and water molecules in the annealed samples crystal structure.

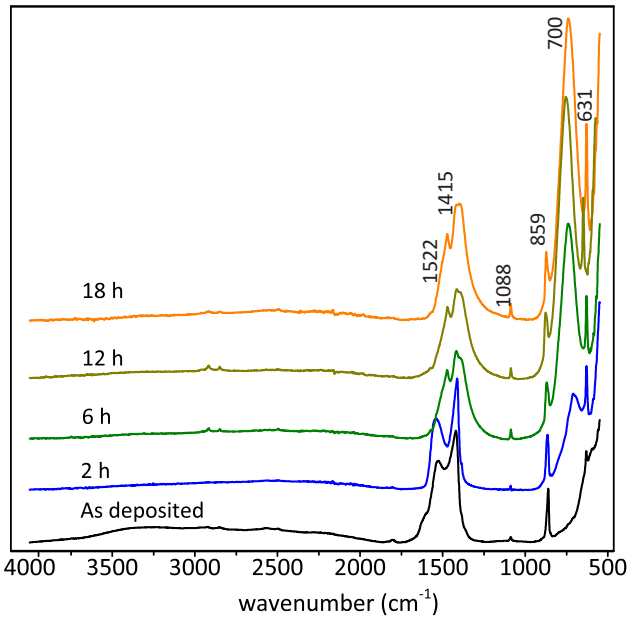

Figure 3: IR spectra collected for Li_2CO_3 for as-deposited samples and samples treated during different annealing times.

Regarding the analysis of the topography of Li_2CO_3, the surface is an important parameter owing the electrochemical reactions that takes place there. An AFM analysis was performed to study the evolution of the Li_2CO_3 surface with the annealing time as Figure 4 shows. The as-deposited samples, Figure 4(a), present a flat arrangement of small

particles in contrast to the particles that appear with longer times. The obtained particles have a pseudo-hexagonal geometry and their size increases with longer annealing times (see SI). These particles are illustrated in Figures 4(b)-(e). The observed particles have an average diameter of 2.8 ± 0.1 μm, 4.3 ± 0.4 μm, 13.0 ± 1.1 μm and 16.8 ± 1.8 μm for the samples treated during 2h, 6h, 12h and 18h, respectively. Moreover, the height of the obtained Li_2CO_3 particles increases between samples and values of 0.65 ± 0.03 μm, 0.79 ± 0.04 μm, 0.93 ± 0.11 μm and 1.16 ± 0.11 μm were obtained. Regarding the surface of the pseudo-hexagonal particles a stepped arrangement is observed as Figure 4(f) illustrates, specially for the samples annealed during 12 h and 18 h. A similar stepped arrangement is observed in calcite crystal grown in presence of Li^+ ions where a rhombohedral cleavage is given.[16] In light of the results, the surface of the particles of monoclinic Li_2CO_3 present a basal cleavage-like growth with a slight tilt. Due to the nucleation and growth of these particles, they present a tilt between 10 º and 15 º, measured from the cross sections of the particles, similar to the values obtained in the bibliography for calcite crystals ($CaCO_3$) in presence of Li^+ ions where similar growing structures have been observed.[17,18] With regards to the geometry of the pseudo-hexagonal particles, all of them present some vertex with a specific angle of 114 º. This angle corresponds to the β angle of the monoclinic unit cell of Li_2CO_3 which could be representing a preferred growing direction of the observed particles. The roughness of the flat material that surrounds the particles, higher than the substrate roughness, indicates that it is a Li_2CO_3 continuous film and the height of the particles might be promoted by the contraction of the film in these particles, making the surrounding films thinner. Moreover, the SEM micrograph shown in Figure 5 confirms this hypothesis showing continuous nanogranular rough film around the particles.[19–24] Unlike the samples of 200 nm Li_2CO_3 the appearance of this specific particles is explained by the thickness of Li_2CO_3 films but also by longer annealing times.

The EIS technique was used to study the influence of the annealing time on the impedance and activation energy of Li_2CO_3 samples. All the samples were tested in a CO_2 atmosphere

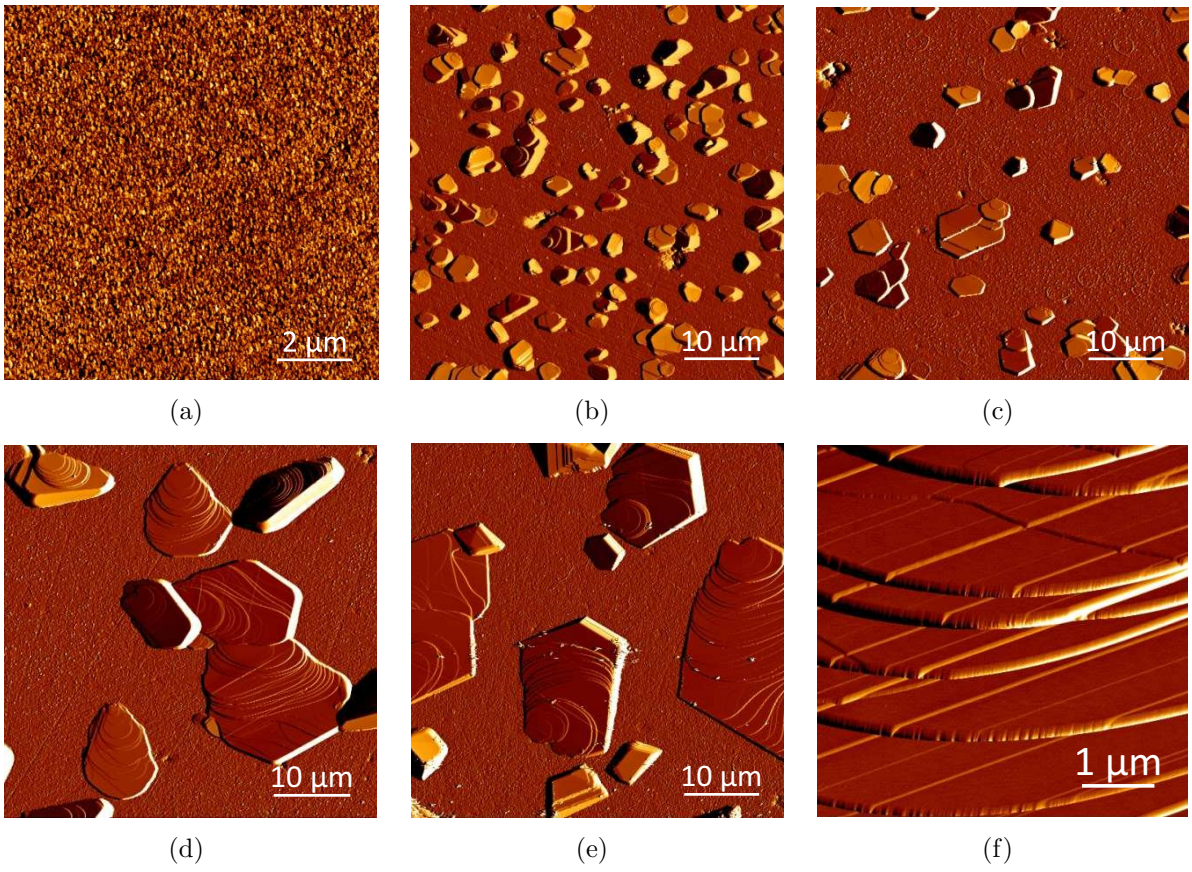

Figure 4: AFM images of (a) as-deposited samples and the samples treated at 600 °C during (b) 2h, (c) 6 h, (d) 12 h and (e) 18 h. (f) A closer image of the stepped arrangement of the particles appeared in the samples treated during 18 h.

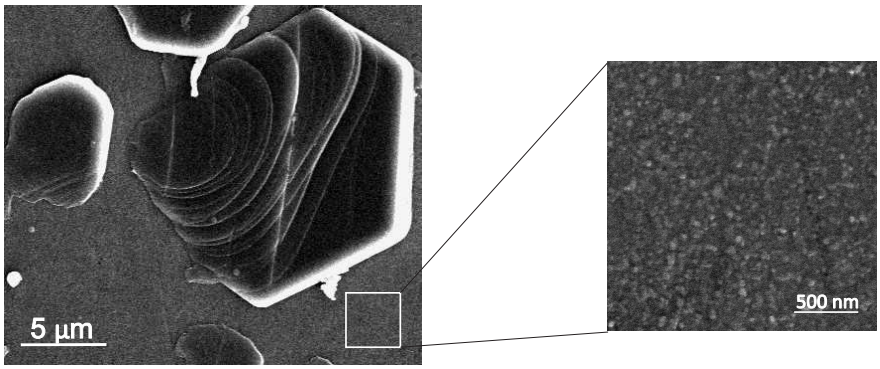

Figure 5: SEM micrograph of the samples treated during 12 h at 600 °C. A continuous film between the particles is observed in the detail picture.

in the temperature range of 200-425 °C. Figure 13(a) shows a detail of a representative measurements obtained in the studied temperature range. The used equivalent circuit that fits the results is shown in Figure 13(b). The complete impedance spectra is shown in Figure 8 in SI.

It is important to note that in all cases the spectra present a two arc graph whose impedance diminishes with the measuring temperature. The high frequency arc (left hand arc in Figure 13(a)) represents the processes related in the conduction through the Li_2CO_3 thin film whereas the low frequency arc represent the reaction in the electrodes. Focusing on the high frequency arc, it gets smaller until it practically disappears at temperatures above 400 °C with an extremely low impedance value. This fact means that the conduction is improved with the test temperature.

Table 1: Impedance value obtained from a sample treated at 600 °C during 2 h, 6 h, 12 h and 18 h.

T.Temp (°C)	R_p (kΩ) 2 h	R_p (kΩ) 6 h	R_p (kΩ) 12 h	R_p (kΩ) 18 h
200	9480.5±26.7	6110.0±10.8	16300.0±77.0	24323.0±49.9
250	454.02±1.07	424.0±0.6	730.0±2.3	634.8±2.3
300	48.80±0.30	58.68±0.07	27.18±0.21	24.96±0.13
350	9.42±0.03	13.66±0.02	5.53±0.01	13.15±0.03
400	2.810±0.004	3.228±0.006	3.276±0.002	4.673±0.007
425	0.2650±0.0003	1.046±0.003	2.5262±0.0008	2.9865±0.001

The equivalent circuit that fits the impedance spectra, illustrated in Figure 13(b) is used to analyze quantitatively the evolution of the impedance with the temperature and, this way, obtain the activation energy of the samples and compare different samples to understand the effect of the microstructure on conduction mechanism. The R_s and the $R_p \| C$ parallel circuit represents the resistance of the connections and the processes related to the conduction through the Li_2CO_3 thin film, respectively. Only the high frequency arc, corresponding to Li_2CO_3, is studied because of the irrelevance of the electrode arc in the Li_2CO_3 conduction mechanism. The values obtained from the fitting of Figure 13(a) are shown in Table 1. As it may be observed, the impedance decreases with the temperature in all cases presenting

a 260 Ω impedance minimum at 425 °C for the samples treated during 2 hours. This low value makes the high frequency arc almost imperceptible compared to the low frequency arc. Samples of 300 nm thick do not present a change of tendency observed around 350 °C in contrast to the samples of 200 nm thick and a minimum impedance at 425 °C is observed. Moreover, comparing the values of the samples treated during 2 hours at 350 °C, the impedance has decreased one order of magnitude from 90 kΩ to 9 kΩ. The decrease on the impedance is explained by the increase of the thickness of the Li_2CO_3 film and decrease of the interdigitated electrodes width and the distance between them, reducing these magnitudes from 50 μm to 25 μm. Interestingly, the impedance evolution with temperature present different behaviour for each annealing treatment. This will be expressed in the obtained activation energy of each sample. Observing the behaviour of C in the Table 2 of the SI, its values remains practically constant for every annealing time at each one of the test temperatures.

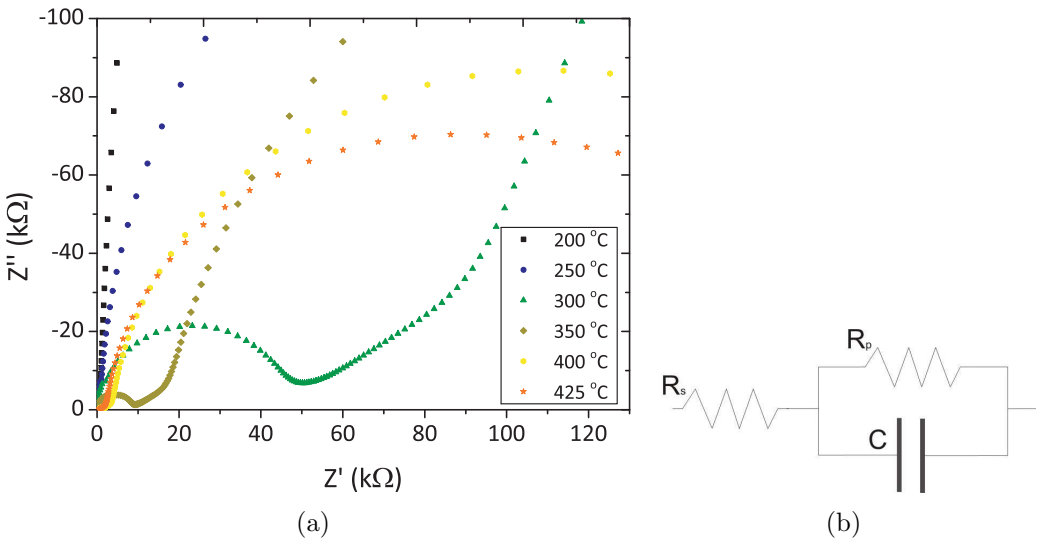

(a) (b)

Figure 6: (a) Li_2CO_3 spectra in the temperature range of 200-425 °C. These spectra corresponds to samples annealed at 600 °C during 2 hours. (b) Electrical equivalent circuit that was used to fit the obtained impedance spectra.

The Arrhenius plot represents the evolution of the impedance of the samples with the temperature. A representative graph obtained for samples annealed at 18 h is depicted in

SI. As the figure illustrates, only one slope is observed which corresponds to the intrinsic region of Li_2CO_3 ionic conductor.[11] This means that the activation energy of the conduction of Li ion through interstitial position[4,25] is a process influenced by the thermally formed new interstitial defects and the migration of the defects. Interestingly, there is a difference between the samples annealed during 2 hours and the rest. The samples treated during 2 hours have an activation energy of 1.26 ± 0.01 eV whereas the samples annealed during 6, 12 and 18 hours have 1.18 ± 0.06 eV, 1.19 ± 0.03 eV and 1.15 ± 0.02 eV activation energies, respectively. Therefore, it can be concluded that the activation energy suffers a decrease for annealing treatments longer than 2 hours but it remains practically the same above six hours. It must be highlighted that these values are lower than the 1.5 eV activation energy obtained from previous work where 200 nm thick samples annealed at 600 °C during 2 hours were studied. Moreover, this values are in agreement with the values calculated by different authors.[26,27] It must be also highlighted, that the obtained values are similar to the one reported for the binary carbonate Li_2CO_3-$BaCO_3$.[28] Therefore, the influence of the thin film thickness and the annealing time is obvious in light of these results. A lower activation energy has been obtained and the operating temperature range has been extended due to the possibility of operating till higher temperatures compared to the 200 nm samples where a 350 °C limit was established.

Conclusions

Several characterization methods have been used (XRD, FTIR, AFM and EIS) to study new sputtered lithium carbonate films that have been subjected to different thermal treatments and that has been fabricated as indicated in earlier work of the group. XRD and FTIR, confirms that the longer annealing times the more crystallinity. However, the crystallite size remains constant.

AFM analysis has shown the appearance of Li_2CO_3 pseudo-hexagonal particles presenting

a maximum diameter of 16.8 ± 1.8 μm and a maximum height of 1.16 ± 0.11 μm. The new sputtered films have presented lower activation energy of 1.15 ± 0.02 eV compared to the 1.5 ± 0.06 eV obtained in previous work. Moreover, 300 nm thick films allow for higher test temperatures (between 200 and 425 °C) without observing a Li_2CO_3 film behaviour decay. This result supposes a new step on the use of Li_2CO_3 thin films as solid electrolyte due to the decrease of the activation energy with respect to the one obtained in previous work or the values simulated in several references. This means a enhancement in the features of the fabricated thin film with respect to the ones fabricated previously.

The crucial factor is the thickness of the Li_2CO_3 layer. It is well known that film thickness affects coating quality and costs and together with longer stabilization times brings Li_2CO_3 films with wider operating temperature range expanding the potential applications of Li_2CO_3 thin films.

Acknowledgement

Funding for this work was provided by the Ministry of Science and Education of Spain within the framework of the NAMIRIS project no. TEC2010-21375-C05-01 “Modular system based on advanced micro and nanotechnologies for safety and air-quality applications”.

Supporting Information Available

Table 2: Impedance value obtained from a sample treated at 600 °C during 2 h, 6 h, 12 h and 18 h.

Test Temperature (°C)	C (F) 2 h	C (F) 6 h	C (F) 12 h	C (F) 18 h
200	2.88×10^{-11}	2.93×10^{-11}	2.80×10^{-11}	3.17×10^{-11}
250	2.60×10^{-11}	2.70×10^{-11}	2.59×10^{-11}	2.77×10^{-11}
300	2.47×10^{-11}	2.59×10^{-11}	2.35×10^{-11}	2.74×10^{-11}
350	2.14×10^{-11}	2.50×10^{-11}	2.92×10^{-11}	2.46×10^{-11}
400	2.32×10^{-11}	2.81×10^{-11}	2.25×10^{-11}	3.32×10^{-11}
425	2.04×10^{-11}	3.87×10^{-11}	2.75×10^{-11}	2.36×10^{-11}

This material is available free of charge via the Internet at `http://pubs.acs.org/`.

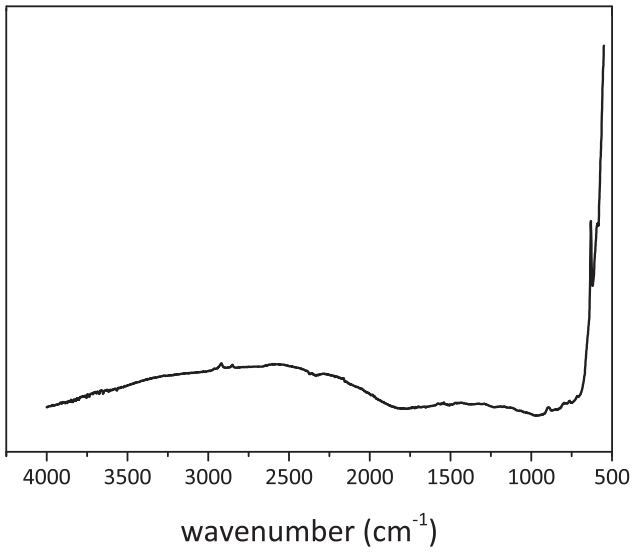

Figure 7: IR spectra of Al_2O_3 substrate.

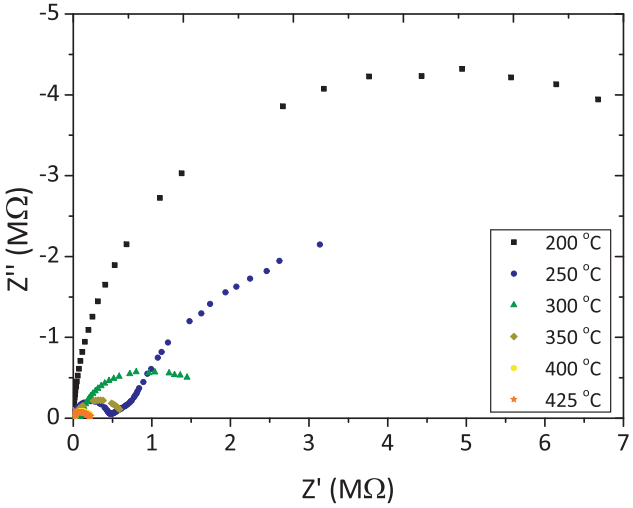

Figure 8: The complete impedance spectra of (Li_2CO_3 thin films.

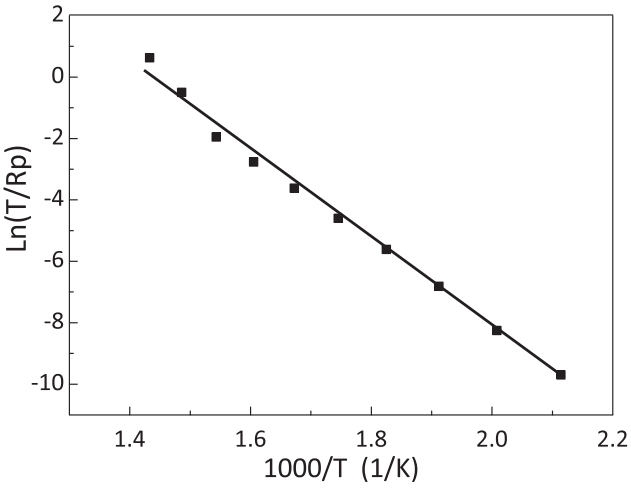

Figure 9: Arrhenius plot of Li_2CO_3 samples annealed at 600 °C during 18 hours. The continuous line represent the performed linear fitting to calculate the activation energy of this sample.

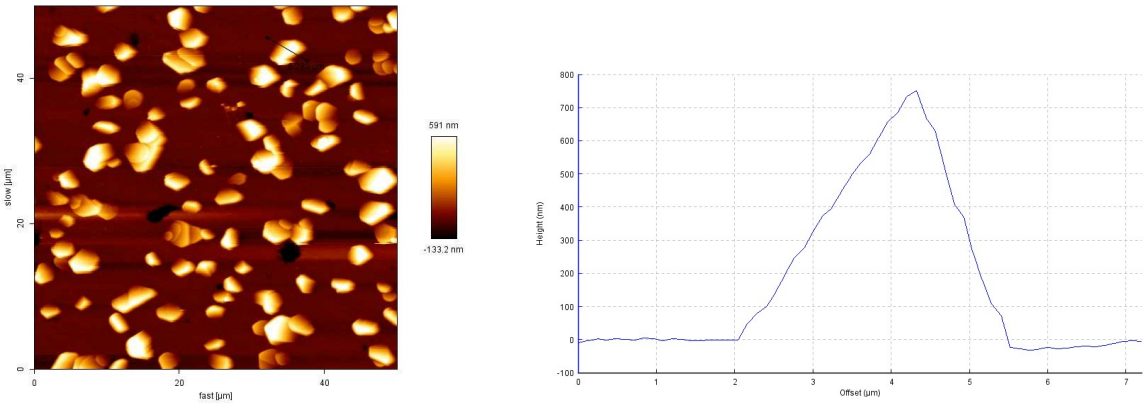

(a) (b)

Figure 10: (a) Height image and (b) cross section of a sample treated during 2 hours at 600 °C.

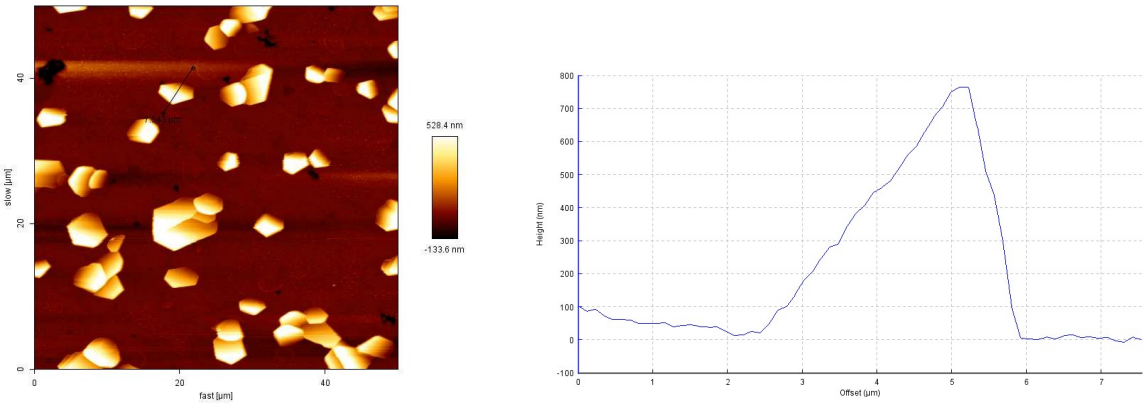

(a) (b)

Figure 11: (a) Height image and (b) cross section of a sample treated during 6 hours at 600 ºC.

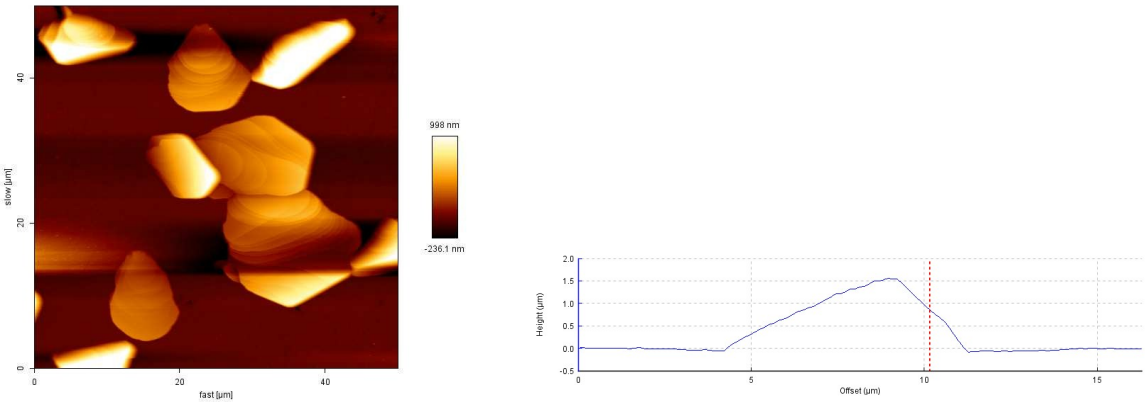

(a) (b)

Figure 12: (a) Height image and (b) cross section of a sample treated during 12 hours at 600 ºC.

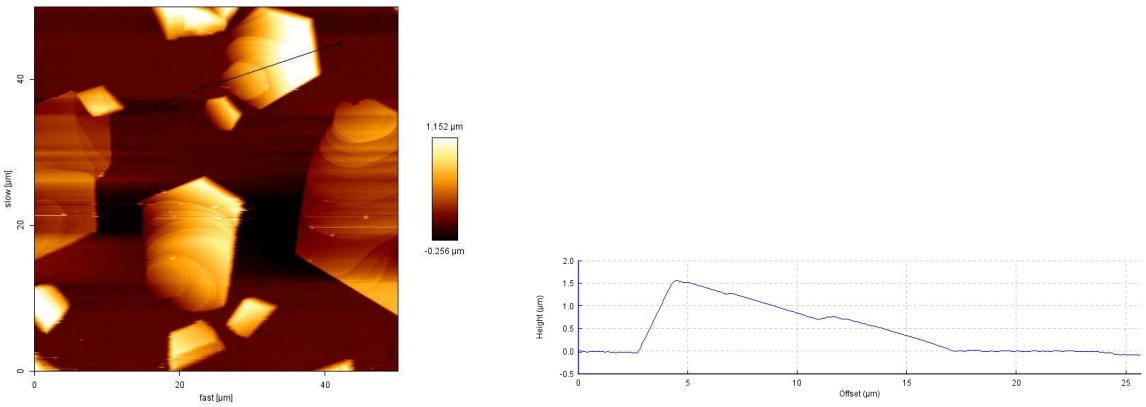

(a) (b)

Figure 13: (a) Height image and (b) cross section of a sample treated during 18 hours at 600 °C.

References

(1) Fergus, J. W. *Sensors and Actuators B: Chemical* **2008**, *134*, 1034–1041.

(2) Park, C. O.; Fergus, J. W.; Miura, N.; Park, J.; Choi, A. *Ionics* **2009**, *15*, 261–284.

(3) Näfe, H. *Sensors and Actuators B: Chemical* **2000**, *69*, 46–50.

(4) Mizusaki, J.; Tagawa, H.; Saito, K.; Uchida, K.; Tezuka, M. *Solid State Ionics* **1992**, *53-56*, 791–797.

(5) Sadaoka, Y. *Sensors and Actuators B: Chemical* **2007**, *121*, 194–199.

(6) Shao, L.; Ma, R.; Wu, K.; Shui, M.; Lao, M.; Wang, D.; Long, N.; Ren, Y.; Shu, J. *Journal of Alloys and Compounds* **2013**, *581*, 602–609.

(7) Shin, J.-s.; Han, C.-h.; Jung, U.-h.; Lee, S.-i.; Kim, H.-j.; Kim, K. *Journal of Power Sources* **2002**, *109*, 47–52.

(8) Zhang, T.; Zhou, H. *Nature communications* **2013**, *4*, 1817.

(9) Pasierb, P.; Komornicki, S.; Rokita, M.; Re, M. *Journal of Molecular Structure* **2001**, *596*, 151–156.

(10) Pasierb, P.; Gajerski, R.; Rokita, M.; Rekas, M. *Physica B: Condensed Matter* **2001**, *304*, 463–476.

(11) Rojo, L.; Castro-Hurtado, I.; Morant-Miñana, M. C.; Mandayo, G. G.; Castaño, E. *CrystEngComm* **2014**, *16*, 6033–6038.

(12) West, W. C.; Whitacre, J.; Ratnakumar, B. V.; Brandon, E.; Blosiu, J. O.; Surampudi, S. **1997**, *791*, 1997.

(13) Xu, X.; Han, J. T.; Kim, D. H.; Cho, K. *The journal of physical chemistry. B* **2006**, *110*, 2764–70.

(14) Roja, T.; Šegedin, P.; Kosec, M. *Using Infrared Spectroscopy to Identify New Amorphous Phases - A Case Study of Carbonato Complex Formed by Mechanochemical Processing, Infrared Spectroscopy - Materials Science, Engineering and Technology*; InTech, 2012; p 510.

(15) Xu, X.; Han, J. T.; Cho, K. *Chemistry of Materials* **2004**, *16*, 1740–1746.

(16) Pastero, L.; Costa, E.; Bruno, M.; Rubbo, M.; Sgualdino, G.; Aquilano, D. *Crystal Growth & Design* **2004**, *4*, 485–490.

(17) Wang, L.; Ruiz-Agudo, E.; Putnis, C. V.; Putnis, A. *CrystEngComm* **2011**, *13*, 3962.

(18) van der Weijden, C.; van der Weijden, R. *Journal of Crystal Growth* **2014**, *394*, 137–144.

(19) Ruffino, F.; Grimaldi, M. G. *Journal of Applied Physics* **2011**, *110*, 044311.

(20) Ruffino, F.; Torrisi, V.; Marletta, G.; Grimaldi, M. G. *Nanoscale research letters* **2011**, *6*, 112.

(21) Ruffino, F.; Torrisi, V.; Marletta, G.; Grimaldi, M. G. *Applied Physics A* **2011**, *103*, 939–949.

(22) Ruffino, F.; Grimaldi, M. G. *Journal of Applied Physics* **2010**, *107*, 074301.

(23) Hirasawa, M.; Shirakawa, H.; Hamamura, H.; Egashira, Y.; Komiyama, H. *Journal of Applied Physics* **1997**, *82*, 1404.

(24) Barreca, D.; Gasparotto, A.; Tondello, E.; Bruno, G.; Losurdo, M. *Journal of Applied Physics* **2004**, *96*, 1655.

(25) Park, M.; Zhang, X.; Chung, M.; Less, G. B.; Sastry, A. M. *Journal of Power Sources* **2010**, *195*, 7904–7929.

(26) Iddir, H.; Curtiss, L. A. *J. Phys. Chem* **2010**, 20903–20906.

(27) Shi, S.; Qi, Y.; Li, H.; Hector, L. G. *Journal of Physical Chemistry* **2013**, *117*, 8579–8593.

(28) Wierzbicka, M.; Pasierb, P.; Rekas, M. *Physica B: Condensed Matter* **2007**, *387*, 302–312.